ENGINEERING TRANSACTIONS • *Engng. Trans.* • **60**, 3, 187–203, 2012
Polish Academy of Sciences • Institute of Fundamental Technological Research (IPPT PAN)
National Engineering School of Metz (ENIM)
SIXTY YEARS OF THE ENGINEERING TRANSACTIONS

2D FE Micromechanics Modelling of Honeycomb Core Sandwich Panels

Charles BETTS, Jianguo LIN, Daniel BALINT, Anthony ATKINS

Head of Mechanics of Materials Division
Department of Mechanical Engineering, Imperial College
Exhibition Road South Kensington London SW7 2AZ
e-mail: Jianguo.Lin@Imperial.ac.uk

A repeating unit cell 2D finite element modelling procedure has been established to model the mechanical behaviour of honeycomb core sandwich panels (e.g. Young's modulus, energy absorbed, etc.). Periodic boundary conditions have been implemented within the model to simulate an infinitely long sandwich panel. An analytical solution using Timoshenko beam theory has been developed to predict the Young's modulus of the honeycomb core, and this has been compared with the FE model results; it is found that there is good agreement between the two values. The FE model can shed light on the mechanics of more complex 3D metal foams.

Key words: micromechanical modelling, sandwich panel, metal foam, honeycomb, finite elements, periodic boundary conditions.

1. Introduction

Metal foams are a relatively new class of materials that show good potential for lightweight structures, energy absorption, and thermal management [1–3]. They are able to combine low density with good bending stiffness and strength [2]. They can also be made with integral skins, which presents the possibility of making composite structures without using adhesive bonding that can be readily formed into curved shapes [4]. They display a densification stage when subjected to a compressive stress, where the stress rises rapidly with strain as the foam cells crush – this has the implication that the integrity of a metal foam core sandwich panel is not necessarily compromised when subjected to impacts. In addition, open-cell foams do not trap moisture (i.e. they are less susceptible to corrosion than honeycomb cores) [5]. Open-cell cores could provide a dual function, and potentially be used for the storage or drainage of fuel [6].

Due to the potential of metal foams, significant efforts have been made to develop analytical as well as finite element modelling techniques for assessing the mechanical properties of foam materials [7–17]. These fall under three categories:

- **Analytical methods**, utilising dimensional analysis that gives the dependence of the foam properties on the relative density but not the cell geometry (e.g. [7]);
- **Finite element methods utilising a repeating unit cell** such as a tetrakaidecahedron. This method can provide the full response of the foam subjected to a stress or strain (e.g. [10]); and
- **Finite element methods utilising the random Voronoi technique**. This approach givers a more accurate representation of the cell geometry of the foams (e.g. [15]).

FE methods are also being developed that utilise a 3D tomographic image (a non-destructive visualisation of a foam at the scale of its cellular microstructure obtained by X-ray tomography) of a real foam as the geometric description of the model (see Fig. 15) [18, 19]. Such techniques could model both open cell as well as closed cell foams and could prove to be useful in predicting the mechanical response of cellular materials.

This paper aims to shed light on the mechanics of complex 3D foams by conducting finite element modelling of 2D regular honeycomb structures. Foams consist of cell walls that form an intricate 3D network which distorts during deformation in ways which are difficult to identify; honeycombs are much simpler. This paper sets out to establish a repeating unit cell 2D finite element modelling procedure to predict the mechanical behaviour of metal foam sandwich panels (e.g. Young's modulus, energy absorbed, etc.). The finite element results are compared to an analytical model developed in Sec. 5 that utilises Timoshenko beam theory to determine the Young's modulus of a honeycomb core.

2. FE model development

2.1. Overview of FE model

Finite element microstructural modelling of regular honeycombs has been conducted in this paper using the software ABAQUS 6.9-1. The model consists of a set area divided into a regular hexagonal tessellation. The honeycomb is enclosed at the top and bottom by solid 0.8 mm thick facesheets to create a sandwich structure. The dimensions of the hexagonal cells were based on those of the open-cell foam ERG Duocel [20]: the strut length was set to 1.5 mm, and the thickness of the struts was set to 0.18 mm [21]. The relative density of the regular hexagon tessellation can be approximated as follows [7]:

$$\frac{\rho^*}{\rho_s} = \frac{2}{\sqrt{3}}\frac{t}{l}\left(1 - \frac{1}{2\sqrt{3}}\frac{t}{l}\right) = 13.4\%, \tag{2.1}$$

where t is the cell wall thickness and l is the strut length (with $t \ll l$).

For practical applications, the thickness of the sandwich panel will be of a specified value in the order of several millimetres. However, the length of the sandwich panel could be up to several metres long; it would be both impractical and computationally inefficient to physically model the full panel length. Therefore, the length of the sandwich panel was progressively increased within the FE model until convergence of the stress-strain plots was achieved so as to identify the smallest length possible that could be modelled while taking into account edge effects. Figure 1 illustrates this principle.

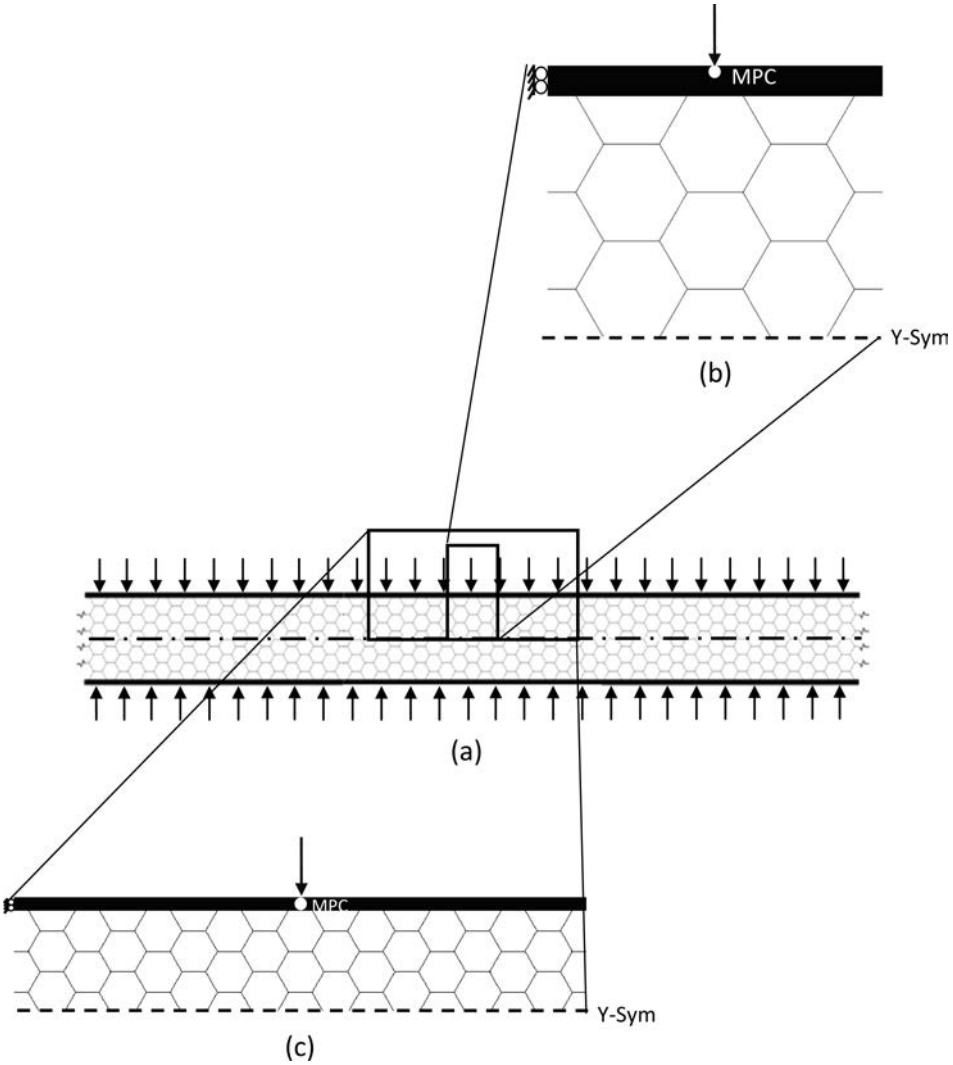

FIG. 1. A sandwich panel structure under uniform loading (a) and its localised micromechanics FE models with different sizes; (b) small size FE model; and (c) larger size FE model.

2.2. Applied boundary conditions and loads

The applied boundary conditions are shown in Fig. 1. A symmetry boundary condition was applied across the horizontal centreline of the sandwich panel. The left face of the upper facesheet was constrained in the horizontal direction.

A uniform compressive load was modelled by applying a multi-point constraint (MPC) along the top face of the upper facesheet, whereby all nodes along that face were tied to the central node. Compressive load vs. displacement plots were obtained by moving this central node in the vertical direction under a controlled, linear displacement.

2.3. Material model

The cell walls of the honeycomb and the facesheets were assigned the material properties of aluminium alloy Al-7075-0: $\rho = 2800$ kg/m^3, $E = 71.7$ GPa, $\sigma_y = 145$ MPa, $\nu = 0.33$. The flow stress was assumed to be given by [20]:

$$\sigma = 400\epsilon^{0.17} \text{ MPa}, \tag{2.2}$$

where σ is the engineering stress, and ϵ the engineering strain.

2.4. Element type, profiles, and time step

The walls of the honeycombs were modelled as beam elements having solid square cross-section. A beam element is a 1D line element in the X-Y plane that has stiffness associated with deformation of the line (the beam's "axis"). These deformations consist of axial stretch/compression and curvature change (bending). The main advantage of beam elements is that they are geometrically simple and have few degrees of freedom.

Specifically, the Timoshenko beam B21 element was used. This allows for transverse shear deformation [23]. For beams made from uniform material, shear flexible beam theory can provide useful results for cross-sectional dimensions up to 1/8 of typical axial distances or the wavelength of the highest natural mode that contributes significantly to the response. Beyond this ratio, the approximations that allow the member's behaviour to be described solely as a function of axial position no longer provide adequate accuracy. ABAQUS assumes that the transverse shear behaviour of Timoshenko beams is linear elastic with a fixed modulus and, thus, independent of the response of the beam section to axial stretch and bending. These elements in ABAQUS are formulated so that they are efficient for thin beams – where Euler-Bernoulli theory is accurate – as well as for thick beams: because of this they are the most effective beam elements in ABAQUS [24].

The B21 element linearly interpolates the displacement field, and hence 15 beam elements were necessary to model each foam strut in order to adequately capture the plastic collapse behaviour of the honeycomb. The upper facesheet was modelled as a shell planar feature comprising of elements of dimensions 0.2×0.2 mm (so, for a model length of 10 mm the upper facesheet comprised of 200 elements). A dynamic, explicit time step was used in order to achieve convergence of the results.

2.5. Connector assignments, constraints, and surface interactions

The foam struts were tied to one another. The joints between the foam struts were constrained in the U1, U2, and U3 translational directions, as well as the UR1, UR2, and UR3 rotational directions. In ABAQUS, this was specified as follows:

- Translational connector type: Join;
- Rotational connector type: Align.

The foam struts at the foam/facesheet interface were tied to the facesheet. Each strut and the facesheet was assigned a tangential frictionless surface interaction property to all part instances in their line of sight.

3. FE results

Figure 2 shows the hexagonal honeycomb stress-strain graph for a relative density of 13.4%, assuming an elastic-plastic material model. The graph displays a trend associated with elastic-plastic honeycombs [7]. There are three distinct regions: a linear-elastic regime, followed by a plateau of roughly constant stress, and finally a regime of steeply rising stress. This behaviour is also typically observed in commercial open-cell foams [2].

The stress-strain behaviour of the honeycombs is described by the different mechanisms of deformation for each region, and can be observed directly from the FE simulations. For the hexagonal honeycomb, the processes are as follows:

1. The cell walls initially bend, resulting in linear-elasticity;
2. Once a critical stress is reached the cells begin to collapse. The cell walls will collapse due to the formation of plastic hinges at the section of maximum moment in the bent members;
3. Finally, the cells collapse to such an extent that opposing cell walls touch one another and further deformation compresses the cell wall material itself. This explains the densification region of the load-displacement graph.

The effect of increasing the length of the sandwich panel can be observed from Fig. 2. As the length is increased from 9 mm to 90 mm, so too is the

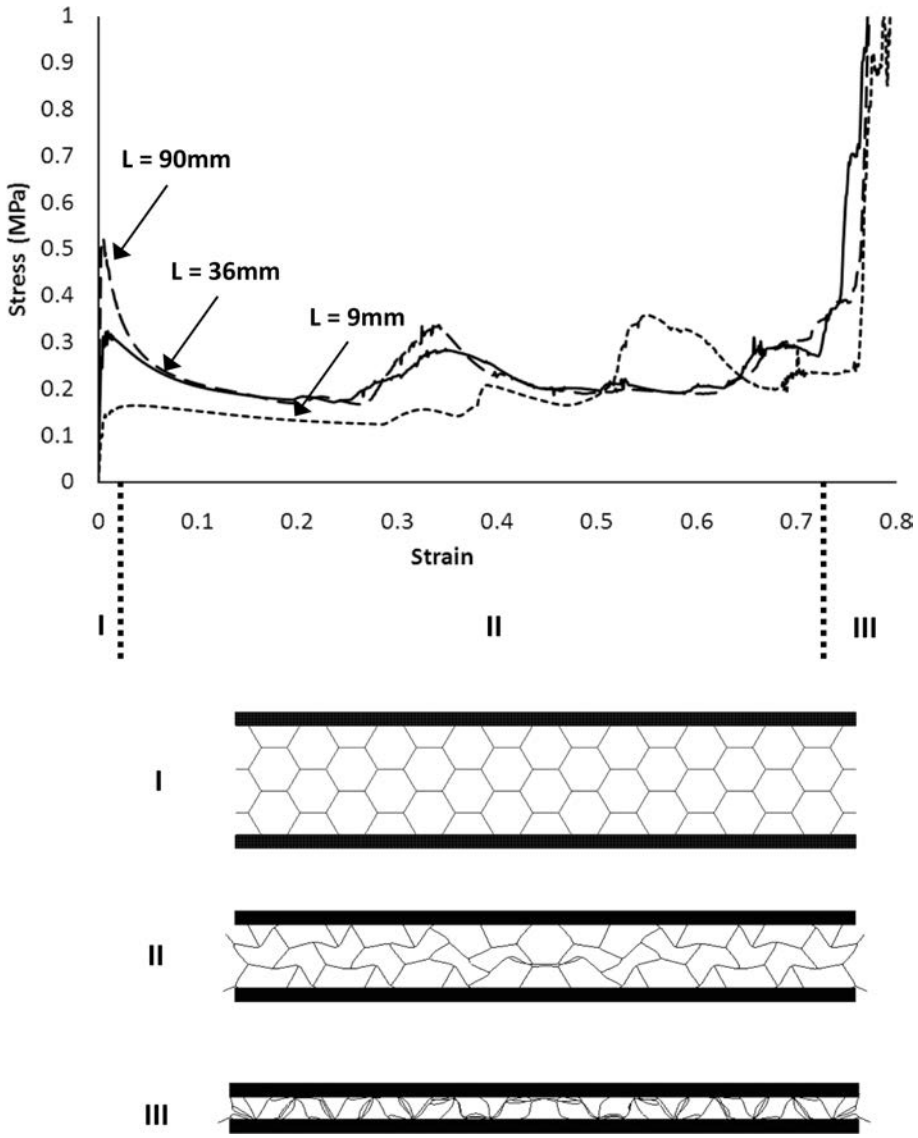

FIG. 2. Nominal stress-strain curves calculated using FE models with different sandwich panel lengths (L). The stress-strain relationships can be divided into three regions as shown: (I) elastic region; (II) plastic collapse followed by plateau; (III) densification.

effective Young's modulus and peak stress. The increase in effective Young's modulus is notable, varying from 36 MPa to 182 MPa. The initial loading peak stress also varies significantly, from 166 kPa to 522 kPa. There is less variation in the plastic properties, and the densification strain is the same for all the models.

As the stress-stain plots do not converge even at a length of 90 mm, it is necessary to investigate implementing periodic boundary conditions at the left and rightmost nodes of the model to describe a sandwich panel of infinite length. This is discussed in Sec. 4.

4. Implementation of Periodic Boundary Conditions

Periodic boundary conditions (PBCs) have been applied to previous FE models of metal foams and honeycombs to simulate an infinite array of cells connected to each other [11, 13, 15]. PBCs effectively eliminate edge effects from the mechanical analysis.

For the 2D case, PBCs assume that for any two corresponding beam nodes on the vertical boundaries of the model, the nodes have the same relative displacement in the vertical and horizontal directions and the same rotational angle in the X-Y plane. This is represented by Eqs. set (4.1).

$$\begin{aligned} U_1^L - U_1^R &= 0, \\ U_2^L - U_2^R &= 0, \\ \emptyset^L - \emptyset^R &= 0, \end{aligned} \tag{4.1}$$

where the superscript L denotes a node on the left vertical boundary, and R is the corresponding node on the right vertical boundary (see Fig. 3). The subscripts 1 and 2 denote the respective degree of freedom (DOF) of the node.

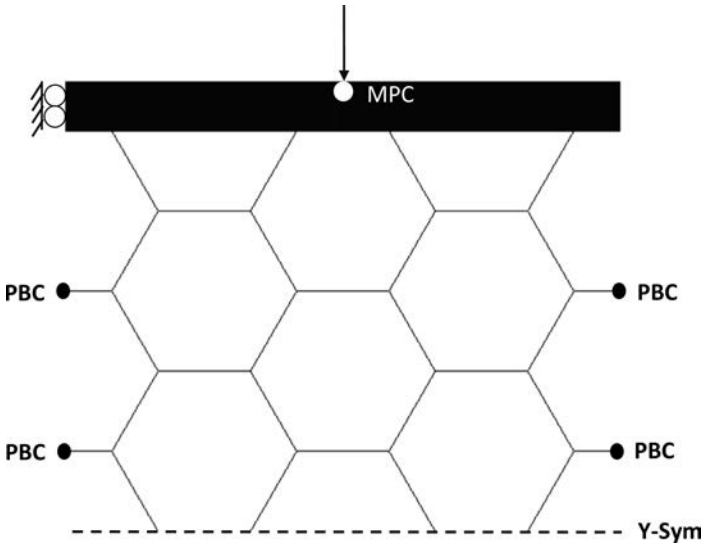

Fig. 3. FE model of hexagonal honeycomb enclosed by metal facesheets, with Periodic Boundary Conditions (PBCs).

The above PBCs were applied to the FE model outlined in Sec. 2, for a facesheet length of 9 mm. PBCs were then applied to the same model for a facesheet length of 45 mm to verify the convergence of the results. Figure 4 shows the stress-strain plots for the two models, and it can be seen that there is a good agreement. The effective Young's modulus varies by 0.2%, whilst the peak stress differs by 0.9% – it is therefore concluded that an infinitely long sandwich panel may be modelled by a facesheet length of 9 mm with PBCs.

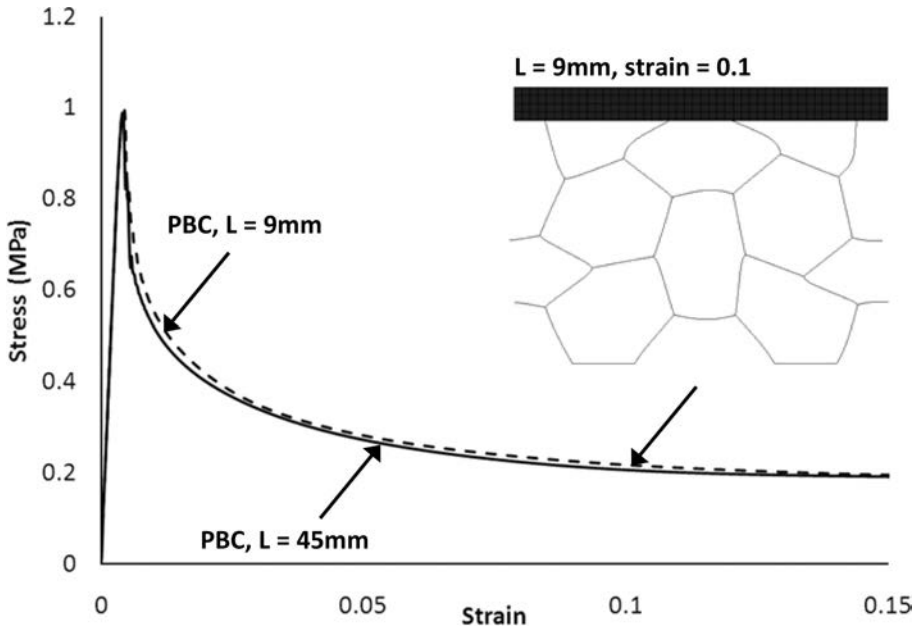

FIG. 4. Comparison of stress-strain relationships calculated using different FE model sizes ($L = 9$ and 45 mm) with PBCs to demonstrate convergence. The deformation for the model length 9 mm at a strain of 0.1 is shown.

4.1. Model convergence

Figure 5 plots the effective Young's modulus and peak stress for the FE models of Fig. 3 – i.e. a facesheet length of 9 mm, 36 mm, and 90 mm without PBCs – and compares these to the value obtained using PBCs as outlined in Sec. 4. It can be ascertained that as the model length increases, it tends towards the solution with PBCs.

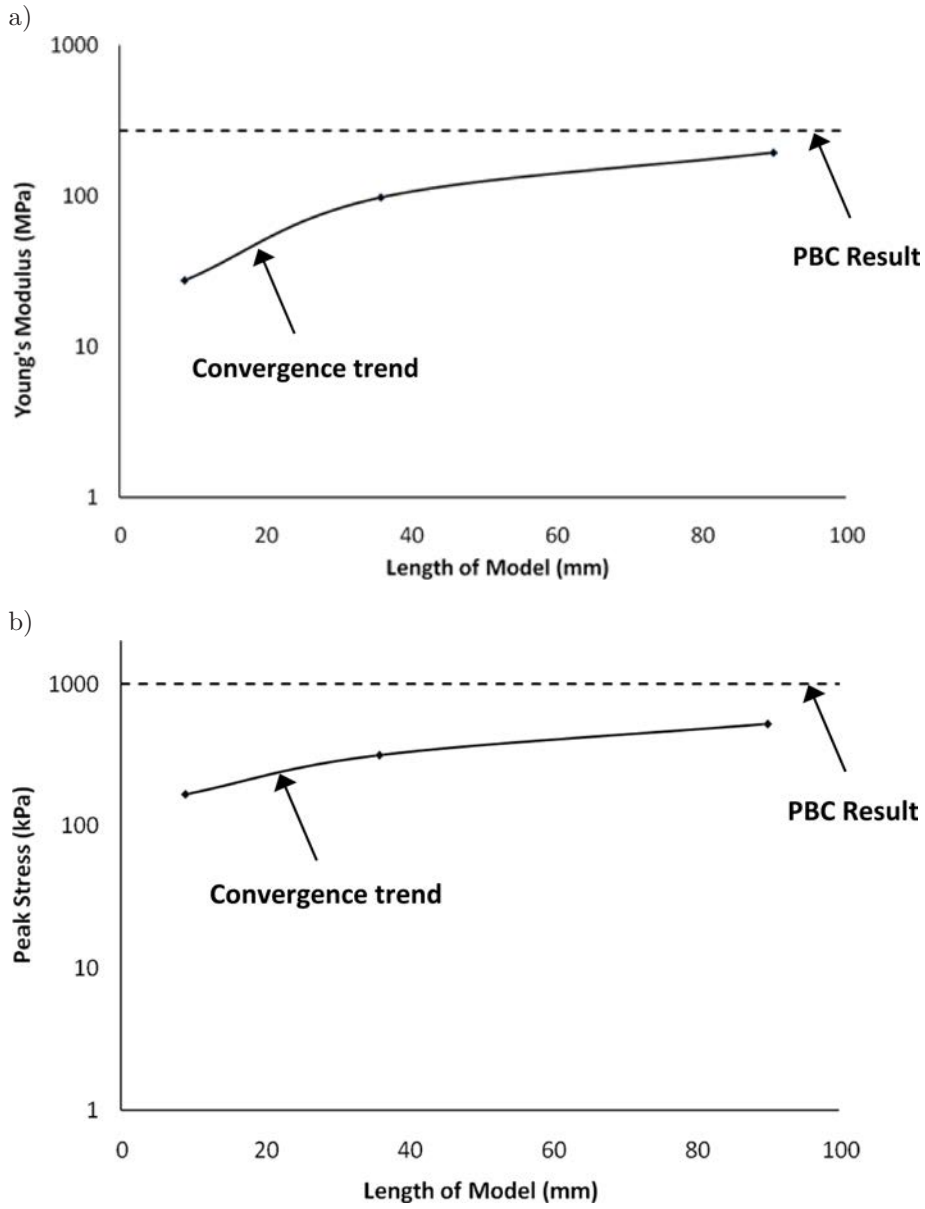

FIG. 5. Convergence of FE models towards PBC solution for: a) Effective Young's modulus and b) peak stress.

5. FE MODEL VALIDATION

ASHBY and GIBSON [7] have previously predicted the Young's modulus of a regular hexagonal honeycomb using Euler-Bernoulli beam theory. In an analogous method to that of [7], Timoshenko beam theory [23] is now used to an-

alytically determine the Young's modulus of a honeycomb in the X_2 direction. Timoshenko beam theory is preferred as it accounts for the effects of transverse shear strain, which are not captured by Euler-Bernoulli beam theory. The latter therefore under-predicts deflections and thus over-predicts beam stiffness. For a homogeneous beam of constant cross-section, Timoshenko beam theory provides the following differential equation to describe the relationship between the beam's deflection and the applied load:

$$E_s I \frac{d^4 w}{dx^4} = q(x) - \frac{E_s I}{kAG} \frac{d^2 q}{dx^2}. \tag{5.1}$$

Consider a honeycomb comprising of regular hexagons of square cross-section and compressed in the X_2 direction, as shown in Fig. 6. By equilibrium, $C = 0$. By separating the load P into components parallel and normal to the beam, the following loading equation for the beam can be written:

$$q(x) = P_n \langle x - 0 \rangle_{-1} - P_n \langle x - l \rangle_{-1} - M \langle x - 0 \rangle_{-2} - M \langle x - l \rangle_{-2}. \tag{5.2}$$

This equation is valid for all values of x from minus infinity to plus infinity, although the beam only exists between $x = 0$ and $x = l$.

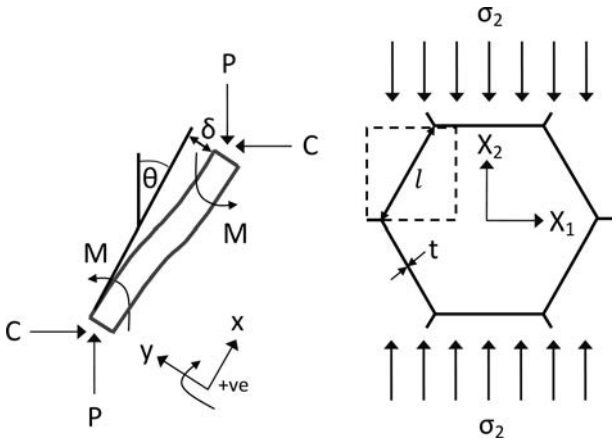

FIG. 6. Free Body Diagram (FBD) of an individual strut subject to uniaxial compression for use in Timoshenko analytical solution.

Inserting the expression for $q(x)$ of Eq. (5.2) into Eq. (5.1) and integrating gives:

$$\begin{aligned} E_s I \frac{d^3 w}{dx^3} &= P_n \langle x - 0 \rangle^0 - P_n \langle x - l \rangle^0 - M \langle x - 0 \rangle_{-1} - M \langle x - l \rangle_{-1} \\ &- \frac{E_s I}{kAG} \left(P_n \langle x - 0 \rangle_{-2} - P_n \langle x - l \rangle_{-2} - M \langle x - 0 \rangle_{-3} - M \langle x - l \rangle_{-3} \right) + C_1. \end{aligned} \tag{5.3}$$

Integrating Eq. (5.3) gives:

$$E_sI\frac{d^2w}{dx^2} = P_n\langle x-0\rangle^1 - P_n\langle x-l\rangle^1 - M\langle x-0\rangle^0 - M\langle x-l\rangle^0 - \frac{E_sI}{kAG}\left(P_n\langle x-0\rangle_{-1} - P_n\langle x-l\rangle_{-1} - M\langle x-0\rangle_{-2} - M\langle x-l\rangle_{-2}\right) + C_1x + C_2. \tag{5.4}$$

The constants C_1 and C_2 can be evaluated by noting that at $x = 0_-$ (i.e. at a point just below $x = 0$):

$$\frac{d^3w(0_-)}{dx^3} = 0 = C_1, \qquad \frac{d^2w(0_-)}{dx^2} = 0 = C_2. \tag{5.5}$$

Integrating Eq. (5.4) twice provides an expression for the slope and deflection of the beam:

$$E_sI\frac{dw}{dx} = \frac{P_n}{2}\langle x-0\rangle^2 - \frac{P_n}{2}\langle x-l\rangle^2 - M\langle x-0\rangle^1 - M\langle x-l\rangle^1 - \frac{E_sI}{kAG}\left(P_n\langle x-0\rangle^0 - P_n\langle x-l\rangle^0 - M\langle x-0\rangle_{-1} - M\langle x-l\rangle_{-1}\right) + C_3,$$

$$E_sI\delta = \frac{P_n}{6}\langle x-0\rangle^3 - \frac{P_n}{6}\langle x-l\rangle^3 - \frac{M}{2}\langle x-0\rangle^2 - \frac{M}{2}\langle x-l\rangle^2 - \frac{E_sI}{kAG}\left(P_n\langle x-0\rangle^1 - P_n\langle x-l\rangle^1 - M\langle x-0\rangle^0 - M\langle x-l\rangle^0\right) + C_3x + C_4. \tag{5.6}$$

The constants C_3 and C_4 can be evaluated by noting that at $x = 0_-$ (i.e. at a point just below $x = 0$):

$$\frac{dw(0_-)}{dx} = 0 = C_3, \qquad w(0_-) = \delta(0_-) = 0 = C_4. \tag{5.7}$$

Hence, from Eq. $(5.6)_2$ at $x = l$ the defection of the beam can be described as follows:

$$E_sI\delta = \frac{P_n}{6}l^3 - \frac{M}{2}l^2 - \frac{E_sI}{kAG}(P_nl - M). \tag{5.8}$$

Now, the moment tending to bend the cell wall is given by:

$$M = \frac{Pl\sin\theta}{2}. \tag{5.9}$$

Inserting Eq. (5.9) in Eq. (5.8), and noting $P_n = P\sin\theta$, gives:

$$E_s I\delta = \frac{Pl^3\sin\theta}{6} - \frac{Pl^3\sin\theta}{4} - \frac{E_s I}{kAG}\left(Pl\sin\theta - \frac{Pl\sin\theta}{2}\right). \tag{5.10}$$

So:

$$|\delta| = \frac{Pl^3\sin\theta}{12E_s I} + \frac{Pl\sin\theta}{2kAG}. \tag{5.11}$$

Now:

$$P = \sigma_2 tl(1+\sin\theta). \tag{5.12}$$

A component $\delta\sin\theta$ of the deflection is parallel to the X_2 axis, giving a strain:

$$\varepsilon_2 = \frac{|\delta|\sin\theta}{l\cos\theta} = \frac{\sigma_2 tl(1+\sin\theta)\sin^2\theta}{\cos\theta}\left(\frac{l^2}{12E_s I} + \frac{1}{2kAG}\right). \tag{5.13}$$

For a beam of square cross-section, $I = t^4/12$ and the Young's modulus is given by (using Eq. (5.13)):

$$E_2^* = \frac{\sigma_2}{\varepsilon_2} = \frac{\cos\theta}{tl(1+\sin\theta)\sin^2\theta\left(\dfrac{l^2}{E_s t^4} + \dfrac{1}{2kAG}\right)}. \tag{5.14}$$

And noting that for a regular hexagon, $\theta = 30°$:

$$E_2^* = \frac{2.3}{\left(\dfrac{l^3}{E_s t^3} + \dfrac{1}{2kG}\right)}. \tag{5.15}$$

For the honeycomb model of Sec. 4, $t = 0.18$ mm, $l = 1.5$ mm, $E_s = 71.7$ GPa, and $G = 27.0$ GPa. The shear coefficient, k, is defined by ABAQUS for a rectangular (or square) cross-section to be equal to 0.85 [24]. So, from Eq. (5.15) $E_2^* = 284$ MPa.

The FE model of Sec. 4, with PBCs, displayed a Young's modulus of 268 MPa, which is in good agreement with the Timoshenko solution (a 6% difference). Figure 7 shows the stress-strain plots for the FE models of facesheet lengths 9 mm, 36 mm, and 90 mm without PBCs, as well as that obtained using PBCs. The Timoshenko analytical solution has been superimposed on the plots.

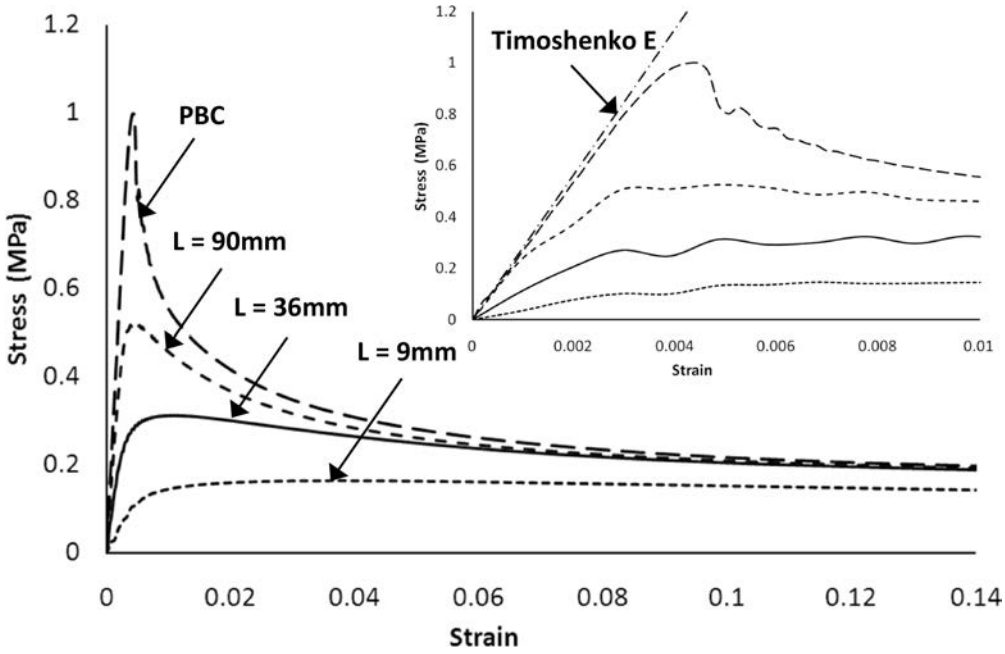

FIG. 7. Comparison of stress-strain plots obtained from different FE model sizes ($L = 9$, 36 and 90 mm) as well as the solution with PBCs. Timoshenko analytical solution is super-imposed to show theoretical Young's modulus in the insert.

5.1. Variance between Euler-Bernoulli and Timoshenko beam theory

For Euler-Bernoulli beam theory, the deflection of a regular hexagonal honeycomb cell wall is given as follows [7]:

$$|\delta| = \frac{Pl^3 \sin\theta}{12E_s I}. \tag{5.16}$$

Comparing this to Eq. (5.11), it is apparent that Euler-Bernoulli beam theory under-predicts deflections. The magnitude of the variation can be expressed by the ratio (for a square cross-section):

$$\frac{\left||\delta|^{\text{Euler}} - |\delta|^{\text{Timoshenko}}\right|}{|\delta|^{\text{Timoshenko}}} = \frac{E_s t^2}{2kGl^2 + E_s t^2}. \tag{5.17}$$

For the FE model of Sec. 4, and varying the beam thickness, this ratio exceeds 10% for values of $t/l > 0.27$. Beyond this value, Euler-Bernoulli beam theory inadequately approximates the deflection of the honeycomb.

Similarly, for Euler-Bernoulli beam theory, the Young's modulus of a regular hexagonal honeycomb cell wall is given as follows [7]:

$$E_2^* = \frac{2.3}{\left(\dfrac{l^3}{E_s t^3}\right)}. \tag{5.18}$$

Comparing this to Eq. (5.15), it is apparent that Euler-Bernoulli beam theory over-predicts the Young's modulus. The magnitude of the variation can be expressed by the ratio (for a square cross-section):

$$\frac{E_2^{*\text{Euler}} - E_2^{*\text{Timoshenko}}}{E_2^{*\text{Timoshenko}}} = \frac{E_s t^3}{2kGl^3}. \tag{5.19}$$

For the FE model of Sec. 4, and varying the beam thickness, this ratio exceeds 10% for values of $t/l > 0.4$ and Euler-Bernoulli beam theory inadequately approximates the Young's modulus of the honeycomb.

6. Relevance to industrial applications

The FE model of Sec. 4 can shed light on the mechanics of more complex 3D metal foams. Indeed, such foams show a similar compressive stress-strain response to the 2D honeycomb structure, with three distinct regions: a linear-elastic regime, followed by a plateau of roughly constant stress, and finally a regime of steeply rising stress [2]. As noted in the Introduction, metal foams can combine low density with good bending stiffness and strength, and are hence attractive as cores of lightweight sandwich structures. Such sandwich structures show promise in the design of aircraft wing boxes, which are at present typically fabricated utilising thin panels that comprise of a skin stiffened by stringers [25]. The resultant panels are light and stiff, but relatively expensive to produce due to high machining costs and the inefficient use of material. Sandwich structures provide a continuous stiffness distribution within the skin panel, which leads to a reduced parts count for assemblies and hence less logistics, parts manufacturing, and assembly work [26]. In addition, open-cell sandwich cores can provide multiple functions and potentially be used for the storage or drainage of fuel within the wings.

It has been ascertained, in Subsec. 5.1, that for values of $t/l > 0.27$, Euler-Bernoulli beam theory inadequately approximates the deflection of a 2D honeycomb structure. X-ray micro-tomography (XMT) scans have been conducted for this paper on individual struts of a commercial open-cell metal foam acquired from BPE International, Germany (a metal matrix composite fabricated from an Al-Zn-Mg-Cu (7xxx series) alloy with TiC particles). From the 3D render

of each scanned strut, and using the imaging software ImageJ, it has been determined that the average strut length and diameter is 1.7 mm and 0.562 mm respectively; i.e. $t/l = 0.33 > 0.27$ (see Fig. 8). Therefore, for this material Timoshenko beam theory is required to accurately predict the deflection of a representative equivalent 2D honeycomb structure.

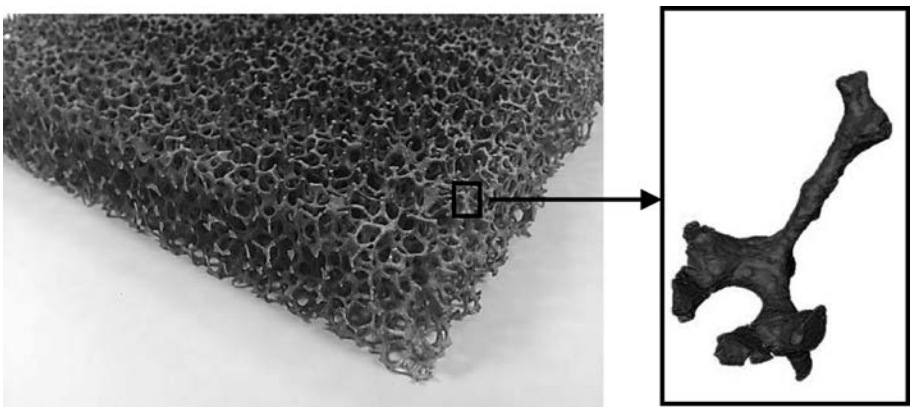

FIG. 8. Morphology of Al-Zn-Mg-Cu foam with TiC particles. The strut dimensions have been determined from XMT scans and imaging software.

Finally, there is scope to conduct FE modelling of other regular tessellated honeycombs (i.e. square and equilateral triangle cell shapes) using the model established in Sec. 4. For a given value of relative density, the energy absorption, initial collapse strength and Young's modulus of sandwich panels constructed from the different cell shapes can be compared, allowing the best choice for lightweight structural applications to be selected.

7. Conclusions

A repeating unit cell 2D finite element modelling procedure has been established in this paper to model the mechanical behaviour of honeycomb core sandwich panels (e.g. Young's modulus, energy absorbed, etc.). Periodic boundary conditions have been implemented within the model to simulate an infinitely long sandwich panel, and to eliminate edge effects from the mechanical analysis. This avoids the need to physically model the actual sandwich panel length, which is advantageous in terms of both the time to construct the model as well as the time to run the model.

The load-displacement plots display three distinct regions: a linear-elastic regime, followed by a plateau of roughly constant stress, and finally a regime of steeply rising stress. This behaviour is also typically observed in commercial open-cell foams.

An analytical solution using Timoshenko beam theory has been developed to predict the Young's modulus of the honeycomb core, and this has been compared with the FE model results; it is found that there is good agreement between the two values. Euler-Bernoulli beam theory is found to be inadequate for predicting the Young's modulus of the modelled honeycomb at values of $t/l > 0.4$, for which Timoshenko beam theory becomes necessary.

The FE model can shed light on the mechanics of more complex 3D metal foams, and could also be used to enable a comparative study of optimal cell shapes for a given application (e.g. energy absorption, lightweight structural applications, etc.).

References

1. Banhart J., *Manufacture, characterisation, and application of cellular materials and metal foams*, Prog. in Mat. Sci., **46**, 559–632, 2001.
2. Ashby M.F., Evans A., Fleck N.A., Gibson L.J., Hutchinson J.W., Wadley H.N.G., *Metal foams: a design guide*, Butterworth-Heinemann, USA 2000.
3. Evans A.G., Hutchinson J.W., Fleck N.A., Ashby M.F., Wadley H.N.G., *The topological design of multifunctional cellular metals*, Prog. in Mat. Sci., **46**, 309–327, 2001.
4. McCormack T.M., Miller R., Kesler O., Gibson L.J., *Failure of sandwich beams with metallic foam cores*, Int. Journal of Solids and Structures, **38**, 4901–4920, 2001.
5. Sypeck D., *Cellular truss core sandwich structures*, Applied Composite Materials, **12**, 229–246, 2005.
6. Wicks N., Hutchinson J.W., *Optimal truss plates*, Int. Journal of Solids and Structures, **38**, 51–65, 2001.
7. Ashby M.F., Gibson L.J., *Cellular solids structure & properties*, Pergamon Press, UK 1998.
8. Onck P.R., Andrews E.W., Gibson L.J., *Size effects in ductile cellular solids: part I modeling*, Int. Journal of Mechanical Sciences, **43**, 681–699, 2001.
9. Chen C., Lu T.J., Fleck N.A., *Effect of imperfections on the yielding of two-dimensional foams*, J. Mech. Phys. Solids, **47**, 2235–2272, 1999.
10. Simone A.E., Gibson L.J., *Effects of solid distribution on the stiffness and srength of metallic foams*, Acta Mater., **46**, 6, 2139–2150, 1998.
11. Hodge A.M., Dunand D.C., *Measurement and modeling of creep in open-cell NiAl foams*, Metallurgical and Materials Transactions, **34A**, 2353–2363, 2003.
12. Shulmeister V., Van der Burg M.W.D., Van der Giessen E., Marissen R., *A numerical study of large deformations of low-density elastomeric open-cell foams*, Mechanics of Materials, **30**, 125–140, 1998.
13. Huang J-S., Gibson L.J., *Creep of open-cell Voronoi foams*, Materials Science and Engineering, **A339**, 220–226, 2003.

14. Silva M.J., Hayes W.C., Gibson L.J., *The effect of non-periodic microstructure on the elastic properties of two-dimensional cellular solids*, Int. J. Mech. Sci., **37**, 1161–1177, 1995.

15. Zhu H.X., Hobdell J.R., Windle A.H., *Effects of cell irregularity on the elastic properties of open-cell foams*, Acta Materialia, **48**, 4893–4900, 2000.

16. Papka S.D., Kyriakides S., *In-plane compressive response and crushing of honeycomb*, J. Mech. Phys. Solids, **42**, 1499–1532, 1994.

17. Gong L., Kyriakides S., Triantafyllidis N., *On the stability of Kelvin cell foams under compressive loads*, J. Mech. Phys. Solids, **53**, 771–794, 2005.

18. Youssef S., Maire E., Gaertner R., *Finite element modelling of the actual structure of cellular materials determined by X-ray tomography*, Acta Materialia, **53**, 719–730, 2005.

19. Maire E., Fazekas A., Salvo L., Dendievel R., Youssef S., Cloetens P., Letang J.M., *X-ray tomography applied to the characterization of cellular materials. Related finite element modeling problems*, Composite Science and Technology, **63**, 2431–2443, 2003.

20. http://www.ergaerospace.com/index.html, (accessed December 2010).

21. Onck P.R., Van Merkerk R., De Hosson T.M., Schmidt I., *Fracture of metal foams: in-situ testing and numerical modeling*, Advanced Engineering Materials, **6**, 429–431, 2004.

22. El-Domiaty A.A., Shabara M.A.N., Al-Ansary M.D., *Determination of stretch-bendability of sheet metals*, Int. J. Adv. Manuf. Technol., **12**, 207–220, 1996.

23. Timoshenko S.P., *Strength of materials: part III, advanced theory and problems*, D. Van Nostrand Co., New Jersey 1956.

24. ABAQUS 6-9.1 User Manual.

25. Worsfold M., *The Effect of Corrosion on the Structural Integrity of Commercial Aircraft Structure*, published in RTO MP-18, 1998.

26. Herrmann A.S., Zahlen P., Zuardy I., *Sandwich Structures Technology in Commercial Aviation*, Sandwich Structures 7: Advancing with Sandwich Structures and Materials, 13–26, 2005.

Received March 18, 2012; revised version August 1, 2012.